International Symposium
On Turbulence and Shear Flow
Phenomena (TSFP-9)
June 30 - July 3, 2015 *Melbourne, Australia*

RICH FLOW PHYSICS IN CURVED ARTERIES AND THE VOCAL TRACT

Michael W. Plesniak[1]
1: Dept. of Mechanical & Aerospace Engineering,
The George Washington University, USA
* Corresponding author: plesniak@gwu.edu

ABSTRACT

Flow in the human body is primarily laminar and pulsatile. Turbulence or transitional flow plays a role in speech production and pathological flows in the circulatory system. Examples of pathological blood flow in which unsteadiness, separation and turbulence are important include regurgitant heart valves, stenoses or blockages, stents, and arterial branches and bifurcations. Speech production involves unsteady pulsatile flow and turbulent structures that affect the aeroacoustics and fluid-tissue interaction. Pulsatile, unsteady phenomena, coherent vortical structures and transitional flow or turbulence occurring at low Reynolds numbers are common to these biological flows. An overarching motivation for studying cardiovascular flow and speech is to facilitate surgical planning, i.e. to enable physicians to assess the outcomes of surgical procedures by using faithful computer simulations. Such simulations are on the horizon with the advent of increasingly more powerful high performance computing and cyberinfrastructure, but they still lack many of the necessary physical models.

INTRODUCTION

The human body is a complex system that is comprised of mechanical and fluid dynamics components performing a range of functions such as delivery of oxygenated blood, voice production, vision, locomotion and blood pressure regulation, etc. Driven by the desire to understand cardiovascular functions and pathologies associated with blood flow within the intricate network of arteries, cardiovascular flows have been of tremendous importance to clinicians and to fluid mechanicians. Similarly, the mechanisms of voice production due to the combined influence of acoustics of vocal tract and mechanical response of the vocal folds present challenging problems associated with laryngeal function and phonatory dynamics. Of particular interest in the latter is flow in pathological situations, such as flow around polyps, or bumps on the vocal fold surface.

Central to the control and functioning of blood flow and voice production aero-hydrodynamics is the persistence of vortices and vortex-induced phenomena. Secondary flow structures are vortical patterns commonly found in curved arteries and form due to a combination of centrifugal instabilities and adverse pressure gradients (Dean, 1927; Dean, 1928; Lyne, 1970). Similarly, the periodic hairpin vortices that form downstream of a surface-mounted hemisphere, a simple model of a polyp, can be associated with Kelvin-Helmholtz instability in a free shear layer (Acarlar and Smith, 1987; Savory and Toy, 1986).

Gaining a mechanistic understanding of the formation, persistence or disruption of vortical structures requires the retention of key physiological parameters and high fidelity flow measurements.

Non-invasive, fundamental experimental investigations were performed in idealized models wherein the complex arterial geometry was represented by a canonical 180-degree curved tube model and the complex geometry of a polyp was replaced simpler surface-mounted hemisphere. These idealized geometries were subjected to pulsatile, physiological inflow conditions, similar to those experienced in large arteries and the vocal tract, respectively.

The analysis of the measured flow fields encompasses the concepts of flow physics, critical point theory and a novel wavelet transform algorithm applied to experimental-data from two-dimensional particle image velocimetry (PIV) and magnetic resonance velocimetry (MRV) techniques for identification of vortical patterns. The application of coherent structure detection methods then revealed several spatio-temporal vortical morphologies attributed to the richness in the flow physics in our bioinspired flow regimes.

APPLICATION OF COHERENT STRUCTURE DETECTION METHODS

Flow regimes encountered in both the curved artery and surface-mounted hemisphere flows possessed unique vortical content. The abstractions of vortices (or coherent structures) as regions of high vorticity and requiring closed or spiraling streamlines are the basis for application and development of coherent structure detection methods. However, streamline topology changes even under simple Galilean transformations such as constant speed translations (Haller, 2005). Jeong and Hussain (1995) and Haller (2005) pointed out the need for methods that are Galilean invariant or remain invariant under coordinate changes of the form $y = qx + at$, where q is a proper orthogonal tensor and a is the constant velocity vector.

Faithful extraction of coherent structures or vortices in experimental (or numerical) data requires access to the velocity gradient tensor (3 x 3 matrix of velocity differentials). Wallace (2009) suggested that without such knowledge fundamental and defining properties of turbulence, such as vorticity dissipation, and strain rates and helicity, couldn't be studied in the laboratory, making simultaneous measurements of two or three velocity components a necessity. The velocity coordinate

differentials can then be calculated using Taylor series expansions, and the velocity gradient tensor (or 2 x 2 matrix) can be adequately populated.

The secondary flow structures encountered in curved artery experiments have been characterized as multi-scale and multi-strength occurrences of swirling, rotation-dominated or strain-dominated vortical structures. This necessitated size-structure-strength considerations to enable accurate coherent structure detection. Wavelet-based, d2-methods and λ_2-methods were employed.

The surface-mounted hemisphere flows produced a horseshoe vortex wrapped around the hemisphere and periodically shedding hairpin vortices downstream. The swirling strength, λ_{ci}-criterion was used to identify coherent structures in these flow fields. A brief description of each of the aforementioned Galilean invariant methods follows.

Continuous wavelet transform (CWT)

A technique based on continuous wavelet transform (CWT) was used to map the vortex topologies in two-dimensional flow field data by repeatedly convolving a Ricker wavelet (as the mother wavelet, ψ) of varying scale. The convolution (or Fourier domain multiplication) of 2D vorticity data with the mother wavelet enables an exhaustive pattern search to characterize the shapes of two-dimensional vortical patterns. The choice of the 2D Ricker wavelet function (eq. 1) was justified by the following guidelines from Farge *et al.* (1990); (i) preservation of the L^2 norm, (ii) admissibility and (iii) good localization and smoothness both in physical and spectral spaces.

$$\Psi(x,y) = \left\{2 - \left(\frac{x}{\sqrt{l}}\right)^2 - \left(\frac{y}{\sqrt{l\varepsilon}}\right)^2\right\} exp\left\{-\left(\frac{\left(\frac{x}{\sqrt{l}}\right)^2 - \left(\frac{y}{\sqrt{l\varepsilon}}\right)^2}{2}\right)\right\} \quad (1)$$

In eq. 1, l is the scale factor and ε controls the wavelet isotropy. The suitability of the 2D- Ricker wavelet for vortical pattern characterization has been elaborately discussed (Kailas and Narasimha, 1999; Schram, C. and Riethmuller, 2001; Varun *et al*., 2008). Our algorithmic approach (PIVlet 1.2) implements wavelet transforms on vorticity data and computes Shannon entropy of the wavelet transformed vorticity ($\tilde{\omega}$) to determine an optimal wavelet scale and the resolution of multi-scale secondary flow structures (Bulusu and Plesniak, 2013; Bulusu, Hussain and Plesniak, 2014). Measurement ensembles of planar cross-sectional vorticity fields (ω) from MRV- and 2D-PIV-data were are interrogated with PIVlet 1.2 to generate wavelet-transformed vorticity fields ($\tilde{\omega}$) (see Figure 3).

λ_2-criterion

According to the λ_2-criterion of Jeong & Hussain (1995), vortices are regions where $\lambda_2(S_2 + \Omega_2) < 0$, where $\lambda_2(A)$ denotes the intermediate eigenvalue of a symmetric tensor A (Wallace, 2009). This criterion defines the cores of vortices as local pressure minima in chosen planes identified as connected regions with two positive eigenvalues of the pressure Hessian (Chakraborty *et al.*, 2005). The MRV measurements yield three-dimensional flow fields, allowing for the complete velocity gradient tensor to be determined. The λ_2-criterion could be computed using these data (see Figure 3).

d_2-criterion

The discriminant of non-real eigenvalues of the velocity gradient matrix (d_2) is a Galilean invariant method, which separates vortices from other structures in the flow (Vollmers, 2001). This method is applicable to both two- and three-dimensional data. Equation 2 is the two-dimensional form of d_2 applied to the averaged velocity field in this study.

$$d_2 = \left(\frac{\partial u}{\partial x} + \frac{\partial v}{\partial y}\right)^2 - 4\left(\frac{\partial u}{\partial x}\cdot\frac{\partial v}{\partial y} - \frac{\partial u}{\partial y}\cdot\frac{\partial v}{\partial x}\right) \quad (2)$$

The d_2-criterion was applied to the phase averaged, two-dimensional PIV data, where in the contours of $d_2<0$, represented regions where vortices reside (see Figure 4).

λ_{ci}-criterion

The swirling strength criterion λ_{ci} of Zhou *et al.* (1999), which is based on the Δ- or *D*-criterion of Chong *et al*. (1990), identifies vortices using the imaginary part of the complex conjugate eigenvalue of the velocity gradient tensor (Wallace, 2009). The swirling strength criterion not only identifies vortices but also determines their strength and local plane of swirling.

Swirling strength provides a Galilean invariant measure of the swirling content in a flow field. The two-dimensional equation for swirling strength is

$$\lambda_{ci} = \mathrm{Im}[eig(\nabla V)] = \frac{1}{2}\mathrm{Im}\left[\sqrt{\left(\frac{\partial u}{\partial x}\right) - \left(\frac{\partial v}{\partial y}\right)^2 + 4\frac{\partial u}{\partial y}\frac{\partial v}{\partial x}}\right] \quad (3)$$

The λ_{ci} criterion was applied to instantaneous, two-dimensional PIV data (see Figure 7).

MOTIVATION FOR INVESTGATION OF BLOOD FLOW IN CURVED ARTERIES

Our cardiovascular flow studies are motivated by clinical evidence of arterial secondary flow structures, observed during patient diagnosis and associated with curved arteries and their pathophysiological conditions (Kilner *et al.* 1993, Sengupta *et al.,* 2008). Known as "spiral blood flow structures" in clinical terms, secondary flow structures are thought to play a protective role in preventing aortic arterial wall damage. The absence of these structures has been linked to carotid atheromatous disease, renal artery stenosis and rapid deterioration of renal function (Bulusu and Plesniak, 2013).

Under physiological inflow conditions, complicated effects, such as asymmetry and spatio-temporal distributions arise. Several strategies were employed to characterize the multiplicity of secondary flow structures of various length scales in curved arteries with different strengths and morphologies. Continuous-wavelet-transform-derived vorticity fields were computed to characterize secondary flow structures quantitatively and objectively (Bulusu, Hussain and Plesniak, 2014).

The richness in physics of these vortical structures and their loss in coherence during deceleration phases suggest several physiological and non-physiological implications related to the blood flow in diseased, stented and stent-fractured conditions.

Experiments were performed using multi-harmonic,

physiological, carotid artery-based inflow conditions (Womersley number = 4.2). Magnetic resonance velocimetry (MRV) and PIV techniques were implemented independently, on a 180-degree curved artery model to investigate spatio-temporal secondary flow structure morphologies.

Description of the 180-degree curved artery test section

A 180-degree tube machined into an acrylic block comprised a curved artery test section with curvature ratio (r/R), 1/7, and was used as an idealized geometry for curved arteries (Figure 1). The main idealizations made are that of arterial rigidity due to the acrylic-based test section and Newtonian behavior of blood (Fung, 1981; Zamir, 2000; Long *et al.,* 2005). The corpuscular nature of blood is encountered where the vessel diameter is of the same order as that of the corpuscles, making the Newtonian assumptions untenable. On the other hand the Newtonian assumption is justifiable where the diameter of the vessel is large, such as the carotid artery and aorta, and particularly in the core regions of flow. The non-Newtonian behavior of blood may well persist in the near wall regions due to variations in hematocrit distribution. The rigid tube model is relevant particularly for the aged population in which cardiovascular disease is most prevalent, where artery distensiblity is less than 10% due to "hardening" of the arteries.

Table 1. PIV experimental parameters for flow in the curved artery model.

Laser	Imaging	Seeding
Nd:YAG	LaVision Imager Intense 10 Hz	Flouro-Max red™
New wave Solo III	1376×1040 pixels, pitch=6.45um	Fluorescent polymer microspheres
Wavelength=532 nm	Nikkor 50mm lens with f#=8	$d_p = 7\ \mu m$
	Flow geometry: 2D-circular, cross-sections parallel to light sheet	
Energy=50 mJ	Temporal resolution: 100 phases in 4 seconds	

The following Newtonian blood analog fluids were used for both MRV and PIV experiments: (i) Glycerol-DI Water (40-60, % by weight) (ii) 79% saturated NaI, 20% pure glycerol, and 1% water (by volume) (Deutsch *et al.*, 2006). Kinematic viscosity of both blood analog fluids were measure using an Ubbelhode viscometer at approximately 25 °C ($\nu = 3.55$ cSt ± 2.8%).

The MRV-technique offers the advantage of three-dimensional velocity field acquisition without requiring optical access or flow markers. Accordingly, the saturated NaI-based, blood analog fluid with refractive index matched to the acrylic test section (1.45 ± 3.4%) was used only for PIV. The physiological carotid artery waveform was reconstructed from ultrasonic flowmeter measurements on the left carotid artery reported by Holdsworth *et al.* (1999).

This waveform was digitized to discrete, evenly spaced time instances (t) spanning a period (T) of 4 seconds and supplied to the test section using a programmable pump (ISMATEC BVP-Z) controlled using a data acquisition card (NI-USB-6229). In Figure 2, the results of flow rate measurements using the carotid artery waveform are shown. Our wavelet decomposition-based approach to detect coherent secondary flow structures was applied to both PIV- and MRV-data, the details of which follow. Table 1 shows the details for PIV system.

An external trigger sent to PIV and MRV computer by pump controlling unit, which determines zero time reference of each pulse. The entire 4 s period is covered by 100 data sets at each 40 ms time step. Each set contains 20 and 100 image pairs for cross-view and top-view measurements, respectively. The top-view plane in the primary flow direction was located 2.5 mm above the center of the pipe and divided in to eight field-of-views (FOVs) with overlapping regions to cover the entire 180º-curved artery model with higher resolution. The velocity vector maps are obtained by applying multi-pass adaptive cross correlation with decreasing size of 128×128 pixels to 32×32 with 50% overlaps. This leads to vector spacing of 0.223 mm and 0.273 mm for cross-view and top-view respectively. The phase-locked ensemble averaged flow field is obtained by applying averaging in each set. The images are acquired and post-processed using DaVis 7.2 software (LaVision Inc.).

Complete description of the MRV technique is beyond the scope of this paper. Details of functional aspects of the MRV technique, including time-resolved flow imaging and Fourier velocity encoding can be found in a paper by Elkins and Alley (2007). Briefly summarizing this paper, under a strong magnetic field, nuclei with non-zero magnetic moments align along the field. Nuclei associated with the tissue precess at the Larmor frequency. The time-varying fields that result from the precession of this transverse magnetization induce voltages in receiver coils, which are then detected by the MR system. Coupled with repeated radio frequency (RF) excitation pulses, time-varying magnetic field gradients and sequence repetition time (TR), particular types of contrast in final images are achieved. Quantitative velocity information can be obtained using the phase of the MR signal.

Summaries of experimental parameters for PIV and MRV are presented in Tables 1 and 2.

Table 2. MRV experimental parameters for flow in the curved artery model.

MRV Imaging
Flow geometry: 3D - 180° curved artery test section
Magnetic field strength: ~ 3 Tesla
Temporal resolution: 40 phases in 4 seconds
Velocity encoding: R/L 80 cm/s, A/P 40 cm/s, S/I 90 cm/s

Results and discussion of flow in the 180-degree curved artery test section

The pulsatile, carotid artery waveform-based inflow conditions in two separate experiments (MRV and PIV) were maintained as shown in Figure 2. Minimal cycle-to-cycle variation was recorded in the several measurements made upstream of the curved artery test section shown in Figure 1. The MRV technique provided a full three-dimensional velocity field with spatial resolution of ≈0.6 mm, whereas the 2D-PIV has a higher spatial resolution of ≈0.459 mm (vector spacing of ≈0.22 mm with 50% window overlap). Moreover, good agreement between the flow rate data from MRV and PIV can be observed, allowing meaningful flow field comparisons.

Cross-sectional fields of vorticity at various locations determined from the MRV measurements at the systolic peak (t/T = 0.18) are shown in Figure 3. The $\tilde{\omega}$-fields at certain locations (45-, 90-, and 135-degree) generated from corresponding PIV measurements are also presented in Figure 3. These $\tilde{\omega}$-fields are the result of an exhaustive pattern search for secondary flow structures and represent multi-scale vortical patterns (Bulusu, Hussain, Plesniak, 2014). The 3D MRV-data facilitates the characterization and contiguity of large-scale, Dean-, Lyne- and Wall-type (D-L-W) vortices. Variation in strengths and scales and vorticity distributions is observed in three dimensions. Quantification of the complete time-varying, 3D geometry of the secondary flow structure is currently being explored within the MRV-data sets.

Figure 4 shows the non-dimensional velocity and negative regions of the d_2 field for top-view and cross-sectional-view PIV measurements at three time steps in deceleration period ($t/T = 0.18, 0.23$ and 0.3). The negative contours of d_2 denote regions of vortical structures in the flow. At maximum flow rate, i.e. peak systole, ($t/T = 0.18$) flow separation associated with adverse pressure gradient induces a large vortical structure at the initial section of the curve in close proximity to the to the inner wall. As the flow develops along the curve (~ 40˚) this large vortical structure bifurcates into two structures and its axis tilts, so that a projection of this structure is seen on the cross-sectional plane. At later time steps during deceleration, the vortical structures move toward the outer wall. At $t/T = 0.23$ the (D-L-W) type vortices deform and lose their strength at these lower flow rates. For more detailed discussion about D-L-W type vortices, see Bulusu and Plesniak, 2013. Figure 4 shows the vortical structure completely separated from the inner wall at $t/T = 0.3$ and the vortical structure at initial section of the curve deflects the primary flow towards the inner wall, which potentially changes hemodynamic wall shear stress distributions. The translation and dilation of secondary flow structures are hypothesized to be driven by a combination of streamwise and cross-stream centrifugal forces along with adverse pressure gradients leading to breakdowns during the systolic deceleration.

MOTIVATION FOR INVESTIGATION OF SEPARATION OVER A MODEL HUMAN VOCAL FOLD POLYP

Vocal fold polyps and nodules are hemisphere-like protuberances which, when formed on the medial surface of the vocal folds, can greatly impair speech. The classical explanation for their effect on voiced speech is based on the added mass of the growth impeding the vibration of the vocal folds (Koizumi, 1993). While added mass is certainly a component of the pathology, a series of studies by Erath and Plesniak (2010, 2012) and Stewart et al. (2104) have shown the presence of vortical structures and separation around a model vocal fold polyp, which can have a substantial effect on voiced speech. These flow features not only affect the jet created by the vocal folds, but also the surface pressure loading on the vocal folds necessary for sustained vibration and speech.

Description flow over hemisphere representing human vocal fold polyp

The experiments were performed in low-speed wind tunnel with a 0.3 m by 0.3 m by 1.2 m acrylic test section as depicted in Figure 5. The wind tunnel has a freestream turbulence intensity of ~1% and an incoming boundary layer roughly an order of magnitude thinner than the characteristic height of the hemisphere, R=15 mm. Two-dimensional PIV data were acquired in two planes shown in Figure 7: the Streamwise Wall Normal (SWN) plane which vertically intersects the centerline of the hemisphere, and the Streamwise Wall Parallel (SWP) plane which is perpendicular to the SWN plane and ~0.1D above the crest of the hemisphere. The PIV system recording parameters are tabulated in Table 3.

Two sets of data were acquired: steady freestream flow and pulsatile freestream flow. The steady flow case was taken with constant velocity freestream (Re_R = 6500, where R is the radius of the hemisphere). In the pulsatile case, the pulsatility was produced with a set of rotating vanes at the exit of the test section (pulsatile inflow waveform and vane position shown in Figure 6). The blockage ratio ranges from 20% in the fully open position to 100% in the fully closed position.

Table 3. PIV experiments parameters for flow over a surface-mounted hemisphere.

Laser	Imaging	Seeding
Nd:YAG	TSI PowerView Plus	LaVision Rocket Fogger
New wave Gemini PIV	2048×2048 pixels,	Glycerol /Water particles
Wavelength=532 nm	Nikkor 105 mm lens with f#=2.8	d_p = 0.2-0.3 μm
Energy=200 mJ		

The PIV data acquisition was synchronized with the rotation of the vanes using an optical encoder. At every 5° of the 180° cycle, 100 PIV realizations were captured and phase averaged. The PIV data were processed and analyzed with LaVision DaVis 8 software.

Results and discussion of flow over a model human vocal fold polyp

Analysis of the steady freestream flow, benchmark case revealed the same structures thoroughly documented in the literature (results not shown for brevity). In the SWN plane a circular concentration of swirling strength was consistently observed at the windward hemisphere-wall junction, which represents the horseshoe vortex wrapped around the hemisphere. The other primary vortical structures around a hemisphere in steady flow, as identified in literature, are periodically shed hairpin-type vortices. These are formed by Kelvin-Helmholtz instability in the curved free shear layer aft of the hemisphere (Acarlar and Smith, 1987; Savory and Toy, 1986).

The pulsatile inflow results are shown in Figure 7. In the SWN plane, circular counter-rotating concentrations of vortical structures were identified by swirling strength. Throughout much of the pulsatile inflow cycle, the primary swirling strength concentration is confined to the recirculation zone aft of the hemisphere. Thus, the distribution of swirling strength at 0° in Figure 7 is representative of phases 0°-75°, as well as 150°-180°. In the SWP plane at 0°, the swirling strength concentration is confined below the shear layer which the measurement plane of PIV does not intersect.

The intensity of the swirling strength increases by a factor of two throughout inflow acceleration, but remains relatively spatially stationary. During deceleration the dynamics of the vortices associated with the swirling strength concentration are much more complex. As the inflow begins to decelerate, around 75°, the vortex begins to move up, away from the wall. The lateral portions of the vortex begin to separate, moving toward either side of the hemisphere. An early point in this motion can be seen in Figure 7 at 90°. As the inflow continues to decelerate, the vortex grows radially and translates upstream, despite the existence of freestream flow at Re_R = 1000 in the opposite direction of its motion. Phases 90° and 100° exemplify this upstream translation and expansion. The upstream motion continues until around 105° when the inflow begins to accelerate again and the vortex is convected downstream; 130° in Figure 7 is a snapshot of this motion downstream. The vortex quickly disappears around 7D downstream and a new vortex begins to form in the recirculation zone.

While there are several idealizations when compared to the work of Erath and Plesniak (2010, 2012) and even more when compared to vocal fold polyp physiology, this work forms a basis for understanding the fluid structures occurring around a human vocal fold polyp. The arch-like structure seen in Figure 7, produced purely by the pulsatile inflow waveform represents one component of the complex fluid dynamics and fluid structure interaction in the human voice. These structures are then shed and dissipate downstream in the accelerating freestream flow. Understanding the dynamics of these structures is a first step in understanding the fluid flow through pathological human vocal folds, specifically those with a unilateral polyp. The effects of inflow velocity cycle amplitude, inflow profile, hemisphere geometry, and the effect of an opposing wall will be explored in future studies.

CONCLUSIONS

The results of two studies inspired by physiological flows – cardiovascular flows in curved arteries and flow over vocal folds with polyps, or growths – were presented. In both cases the pulsatile inflow conditions resulted in rich viscous flow phenomena, and formation of interesting vortical secondary flows. We have developed a new wavelet-transform based coherent structure detection technique that does not require subjective user-set thresholds. In the curved artery case, representative results were presented from two experiments conducted in different facilities – one utilizing PIV and the other molecular resonance velocimetry (MRV). Although the achievable spatial resolution of the latter is limited, in combination with the PIV results, this facilitates full three-dimensional depiction of the complex vortical structures. The flow over a polyp-like bump revealed a set of novel vortical structures formed under the pulsatile inflow conditions. A set of arch-like structures forms throughout the acceleration phase of the cycle and undergoes upstream translation and radial expansion during the deceleration phase. Our motivation for studying cardiovascular flow and speech is to facilitate surgical planning, i.e. to enable physicians to assess the outcomes of surgical procedures by using faithful computer simulations. Understanding the flow physics is a necessary prerequisite to enable such computational models to be developed.

ACKNOWLEDGEMENTS

This material is based in part upon work supported by the National Science Foundation (CBET-0828903, CBET-1236351), and GW Center for Biomimetics and Bioinspired Engineering (COBRE). A special thanks to the following researchers in the Biofluid Dynamics Lab for their invaluable contributions to this paper: Dr. Kartik Bulusu, Ian Carr, and Reza Najjari. Thank you also to our collaborators at Sanford University on the MRV measurements, Prof. John Eaton and Dr. Chris Elkins.

REFERENCES

Acarlar, M.S., & Smith, C.R., 1987, "A study of hairpin vortices in a laminar boundary layer. Part 2. Hairpin vortices generated by fluid injection," *J. Fluid Mechanics*, **175**(1), 43.

Bulusu, K.V. and Plesniak, M.W., 2013, "Secondary flow morphologies due to model stent-induced perturbations in a 180° curved tube during systolic deceleration," *Experiments in Fluids*, **54**(3): 1493.

Bulusu, K.V., Hussain, S. and Plesniak, M.W., 2014, "Determination of secondary flow morphologies by wavelet analysis in a curved artery model with physiological inflow," *Experiments in Fluids*, **55**, 1832.

Chakraborty, P., Balachandar, S. and Adrian, R.J., 2005, "On the relationships between local vortex identification schemes," *J. Fluid Mech.* **535**, 189.

Chong, M.S., Perry, A.E., and Cantwell, B.J., 1990, "A general classification of three-dimensional flow fields," *Phys. Fluids A* **2**, 765.

Dean, W. R., 1927 "Note on the motion of fluid in a curved pipe," *Phil. Mag.* **20**: 208–223.

Dean, W. R., 1928, "The streamline motion of fluid in a curved pipe," *Phil. Mag. (7)* **5**: 673–695.

Deutsch, S., Tarbell, J. M., Manning, K.B., Rosenberg, G. and Fontaine, A.A, 2006, "Experimental fluid mechanics of pulsatile artificial blood pumps," *Ann. Rev. Fluid Mech.* **38**, 65–86.

Elkins, C.; Alley, M.T., 2007, "Magnetic resonance velocimetry: applications of magnetic resonance imaging in the measurement of fluid motion," *Experiments in Fluids* **43**(6): 823–858.

Erath, B.D., & Plesniak, M.W., 2010, "Viscous Flow Features in scaled-up physical models of normal and pathological vocal phonation," (invited) *International Journal of Heat & Fluid Flow*, **31**, Issue 3, 468-481.

Erath, B.D., & Plesniak, M.W., 2012, "Three-dimensional laryngeal flow fields induced by a model vocal fold polyp," *International Journal of Heat and Fluid Flow*, ***35***, 93–101.

Farge, M., Guezennec, Y., Ho, C.M. and Meneveau, C, 1990, "Continuous wavelet analysis of coherent structures," *CTR, Proc. Summer Program*. 331–348.

Fung, Y.C., 1981, "Mechanical properties of living tissues," New York: Springer, 468p.

Haller, G., 2005, "An objective definition of a vortex. *J. Fluid Mech.* **525**, 1–26.

Holdsworth, D.W., Norley, C.J.D., Frayne, R., Steinman, D.A. and Rutt, B.K, 1999, "Characterization of common carotid artery blood-flow waveforms in normal human subjects," *Physiol. Meas.* **20**(3), 219–240.

Jeong, J. and Hussain, F., 1995, "On the identification of a vortex," *J. Fluid Mech.* **285**, 69.

Kailas, S.V. and Narasimha, R., 1999, "The eduction of structures from flow imagery using wavelets. I - The mixing layer," *Exp Fluids.* **27**(2), 167–174.

Kilner, P.J., Yang, G. Z., Mohiaddin, R.H., Firmin, D.N. and Longmore, D.B., 1993, "Helical and retrograde secondary flow patterns in the aortic arch studied by three-directional magnetic resonance velocity mapping," *Circulation* **88**: 2235–2247.

Koizumi, T., Taniguchi, S., & Itakura, F., 1993, "An analysis-by-synthesis approach to the estimation of vocal cord polyp features," *The Laryngoscope*.

Long, J. A, Undar, A., Manning, K. B., and Deutsch, S., 2005, "Viscoelasticity of pediatric blood and its implications for the testing of a pulsatile pediatric blood pump," *American Society for Artificial Internal Organs*, **51**, 563–566.

Lyne, W., 1970 "Unsteady viscous flow in a curved pipe," *J. Fluid Mech.* **45**, 13–31.

Mittal, R., Erath, B. and Plesniak, M.W. 2013, "Fluid dynamics of human phonation and speech," *Ann. Rev. Fluid Mech.***45**: 437-467.

Savory, E., & Toy, N., 1986, "The flow regime in the turbulent near wake of a hemisphere," *Experiments in Fluids*, *188*, 181–188.

Schram, C. and Riethmuller, M.L., 2001, "Vortex ring evolution in an impulsively started jet using digital particle image velocimetry and continuous wavelet analysis," *Meas Sci Tech.* **12**, 1413.

Sengupta, P.P., Burke, R., Khandheria, B. K. and Belohlavek, M., 2008, "Following the flow in chambers" *Heart Failure Clin*., **4**:325–332.

Stewart, K.C., Erath, B.D., and Plesniak M.W. 2014 "Investigating the three-dimensional flow separation induced by a model vocal fold polyp," *Journal of Visualized Experiments*, **84**, e51080.

Varun, A.V., Balasubramanian, K. and Sujith, R. I., 2008, "An automated vortex detection scheme using the wavelet transform of the d2 field," *Exp Fluids.* **45**, 857–868.

Vollmers, H., 2001, "Detection of vortices and quantitative evaluation of their main parameters from experimental velocity data," *Measurement Science and Technology*, **12**, 1199–1207.

Wallace, J.M., 2009, "Twenty years of experimental and direct numerical simulation access to the velocity gradient tensor: What have we learned about turbulence?" *Phys. Fluids* **21**, 021301.

Zamir, M., "The physics of pulsatile flow," Springer-Verlag Inc., New York

Zhou, J., Adrian, R. J., Balachandar, S. and Kendall, T. M., 1999, "Mechanisms for generating coherent packets of hairpin vortices in channel flow," *J. Fluid Mech.* **387**, 353.

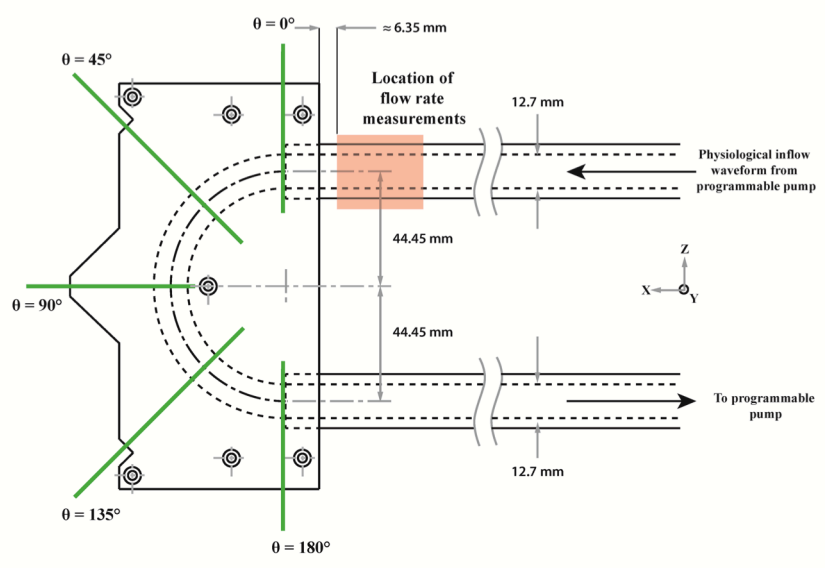

Figure 1. Schematic drawing of the 180° curved artery test section used in 2D-PIV and MRV experiments.

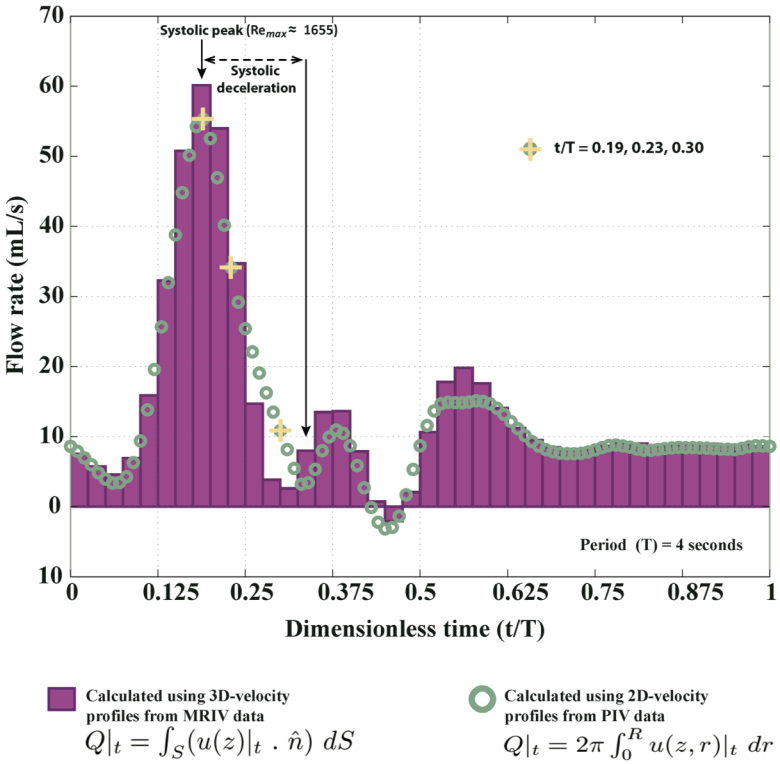

Figure 2. Flow rate measurements from carotid artery-based inflow conditions; green bars (MRV-data in X-Y plane), red circles (2D-PIV-data in X-Z plane).

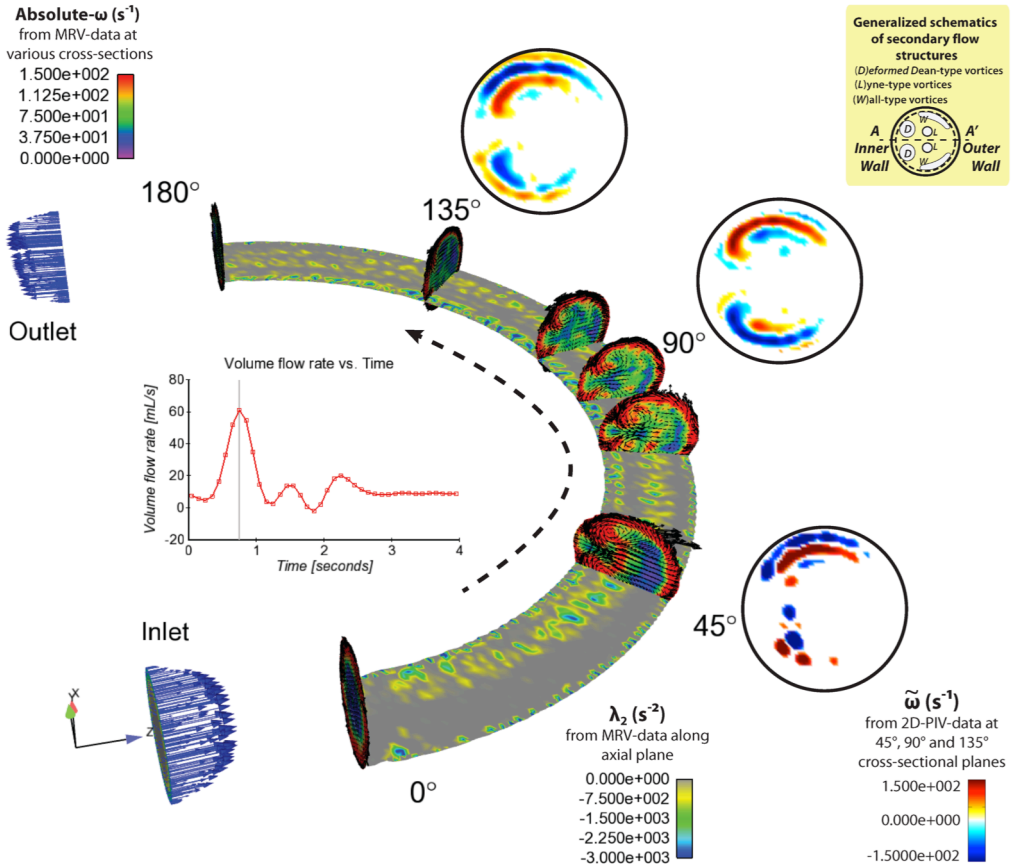

Figure 3. PIV and MRV-data Vortical structure identification (λ_2) and wavelet-transformed vorticity fields ($\tilde{\omega}$).

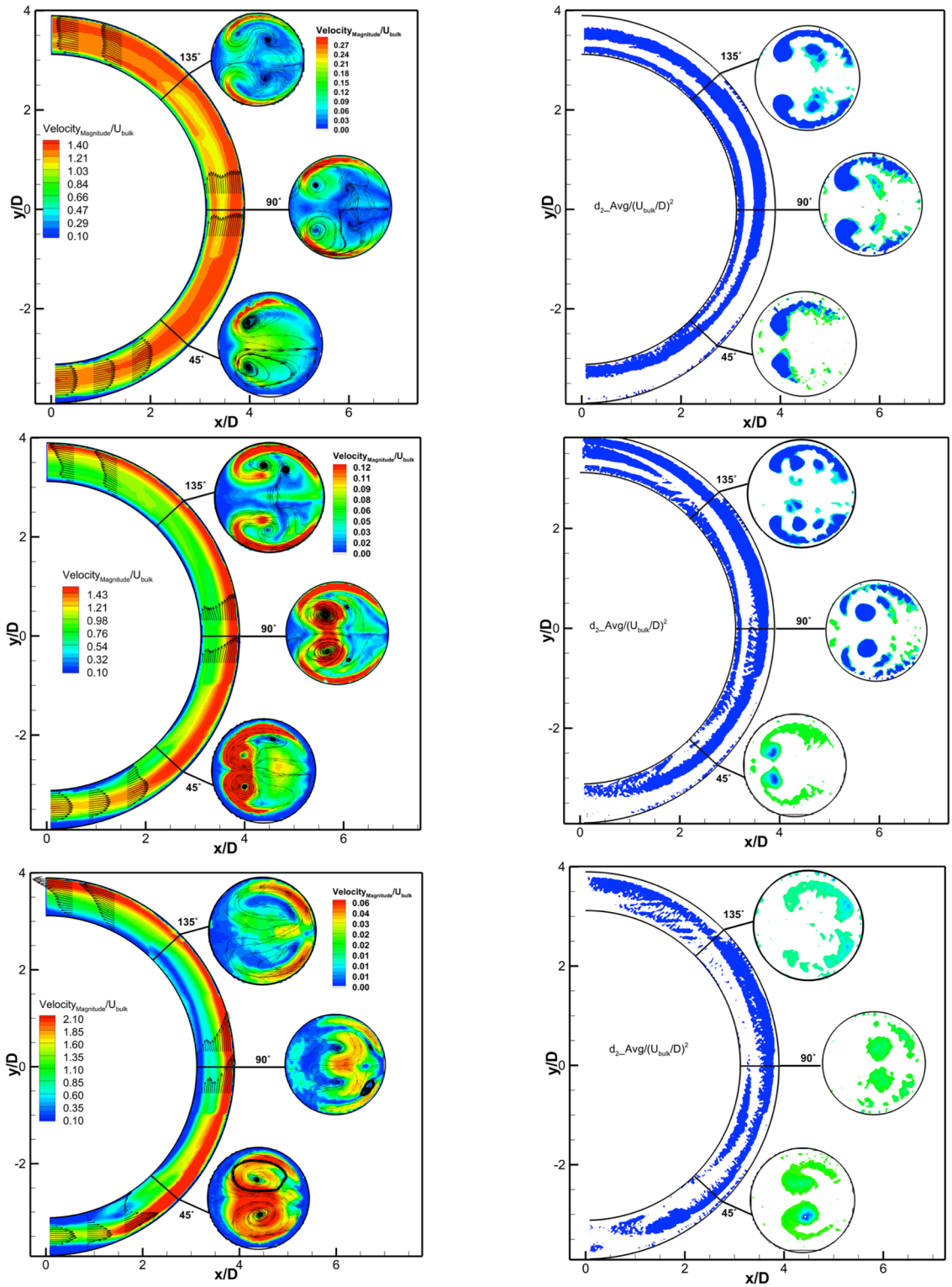

Figure 4. Phase-averaged velocity (left) and d_2 (right) maps at three instances in decelaration t/T=0.18 (top), t/T=0.23 (middle) and t/T=0.3 (bottom).

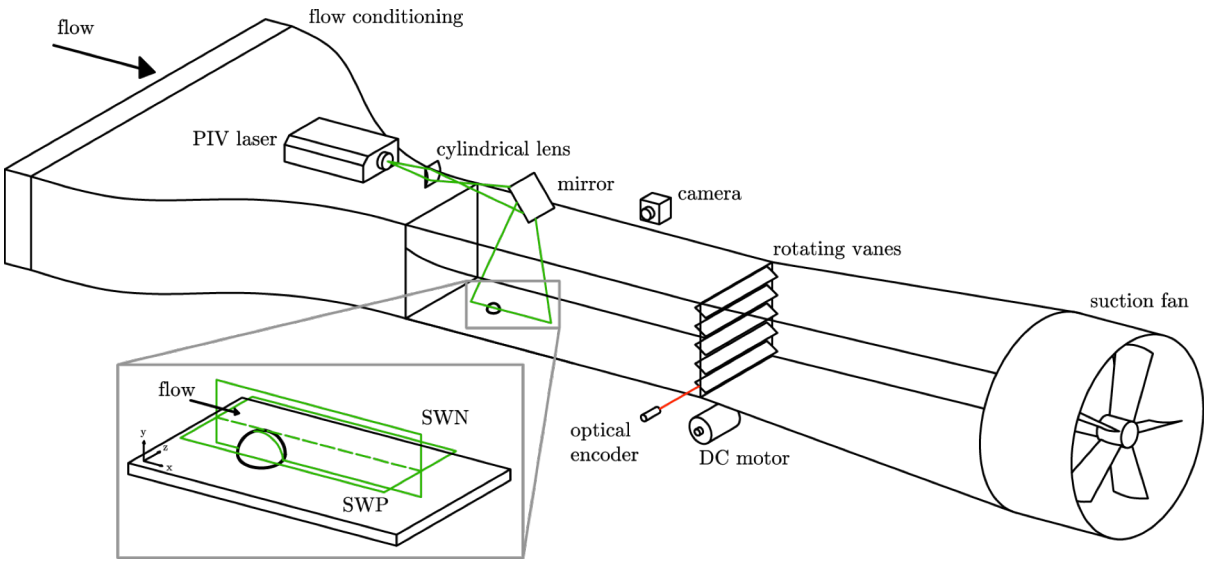

Figure 5. Pulsatile inflow wind-tunnel and PIV planes

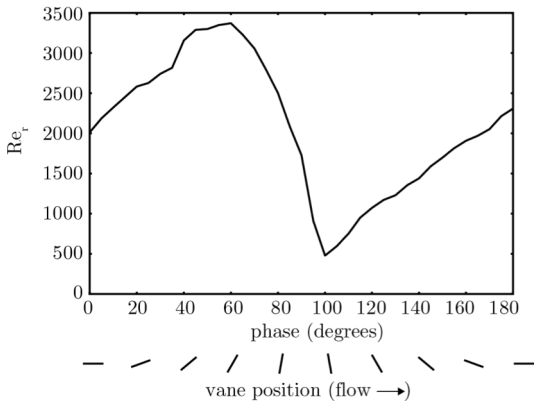

Figure 6. Pulsatile inflow profile and corresponding vane position

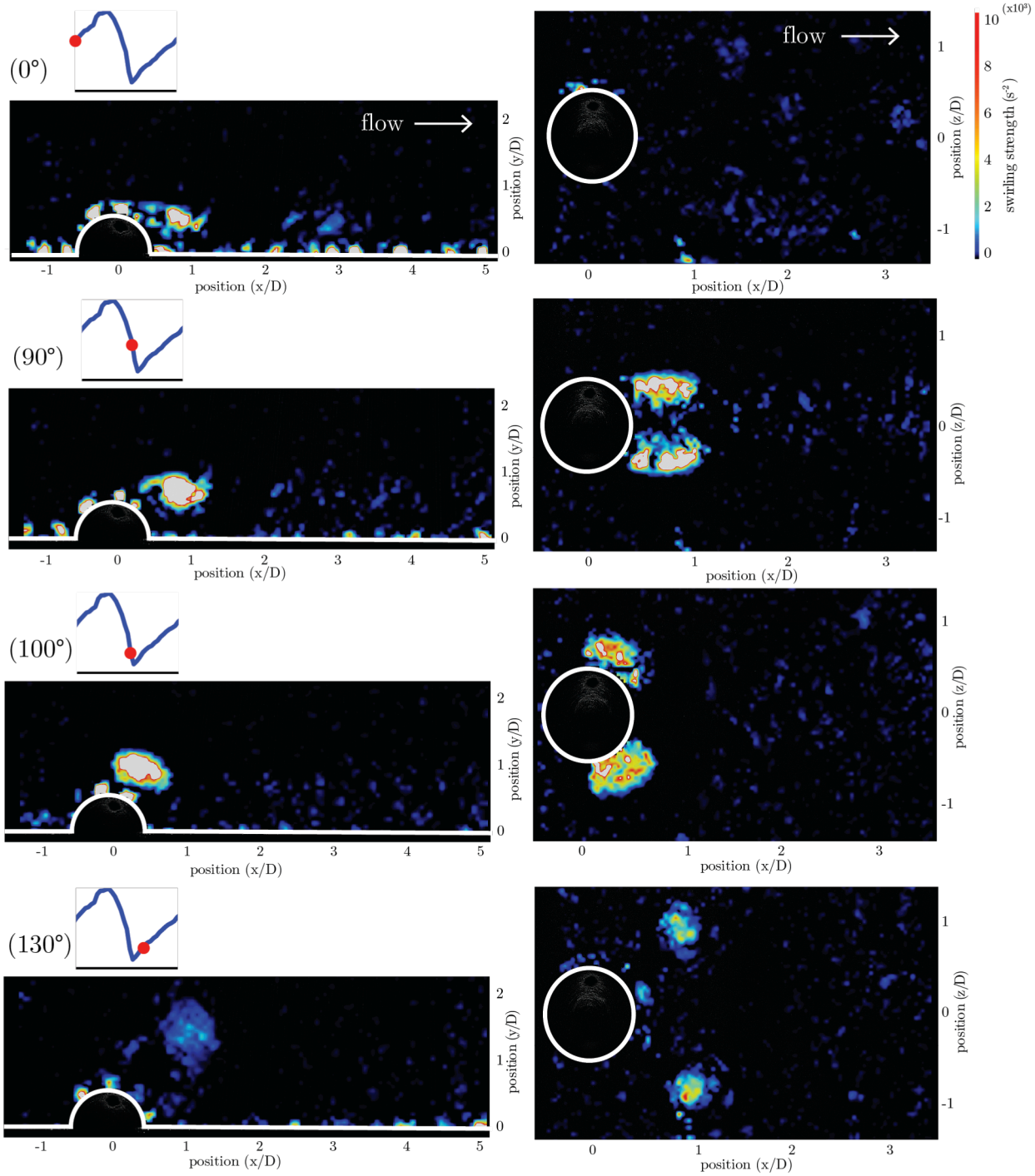

Figure 7. λ_{ci} contours computed from phase-averaged PIV in the SWN plane (left) and the SWP plane (right).